Study the optical parameters of aluminum doped ZnS films deposited on soda-lime glass substrate

A. A. Ahmed [a,*], M. H. Eisa[a,b], M. D. Abdulla[a]
[a]*Department of Physics, College of Science, Sudan University of Science and Technology, Khartoum 11113, Sudan*
[b]*Department of Physics, College of Sciences, Imam Mohammad Ibn Saud Islamic University (IMSIU), Riyadh 13318, Saudi Arabia*

Zinc Sulfide (ZnS) thin films have gained popularity due to their potential field applications. ZnS doped with various elements is redefining academic and industrial research. Pulsed laser deposition (PLD) was applied in the deposition process of undoped ZnS and aluminum (Al) doped zinc sulfide (AZS) on cleaned soda lime glass substrates. The doping effects of aluminum concentration (0, 2, 4, and 6%) on the characteristics of ZnS films were investigated. The ZnS and AZS thin films exhibited a direct allowed bandgap in the range of 3.40 to 3.56 eV, The band gap has been observed to be higher (3.56 eV) indicating blue shift. The linear optical parameters such as oscillator energy (E_0), dispersion energy (E_d), and static refractive index (n_0) were calculated using Wemple and DiDominco's model to find the nonlinear optical susceptibility χ^3 and nonlinear refractive index n_2. The increasing nonlinear parameters χ^3 and n_2 suggest nonlinear optical applications for AZS. The experimental methods and results are described, and the results are compared to published data.

(Received March 3, 2022; Accepted September 8, 2022)

Keywords: ZnS thin films, Optical susceptibility, AZS, Static refractive index, PLD

1. Introduction

Inorganic nanostructures and thin films have been established recently been studied for nanotechnology [1]. Inorganic nanoparticles have recently gained popularity due to their unique properties [1]. Zinc sulfide (ZnS) is a nanomaterial with potential for optoelectronic applications [2]. ZnS is a naturally occurring salt that is non-toxic, non-flammable, and chemically stable. While temperatures seem to be low, ZnS semiconductor materials form cubic zinc-blend (sphalerite) and at high temperatures, wurtzite [4–6]. The bandgap of ZnS is 3.54–3.91 eV for zinc-blend and wurtzite crystalline structures [6,7]. At room temperature, ZnS has a high transmittance, dielectric constant, and refractive index [7,10]. The high processing costs, weight, and fragility of today's cell materials present new challenges. Alternative, low-cost, nontoxic, reliable, and eco-friendly materials like ZnS are required. Thus, ZnS nanoparticles have been used for label-free, real-time, sensitive species detection. Due to its wide direct band gap, ZnS is a promising new UV detector material.

Changing the presence of dopant can change the composition of ZnS [11-13]. Impurity-doped ZnS has different properties than undoped ZnS. Aluminum (Al), indium (In), chromium (Cr), gallium (Ga), fluorine (F), copper (Cu), chlorine (Cl), boron (B), and manganese (Mg) seem to be dopants that could be used to modify the features of ZnS [11-15]. AZS films have excellent properties among doped ZnS materials [13-15]. So, different Al concentrations in ZnS nanomaterials are studied [14,15]. ZnS's optical properties nanomaterials deposited on soda-lime glass substrate has been investigated extensively [15].

Soda-lime glasses are cheap and effective. Aluminum is a popular dopant due to its low cost and small ionic radius. To optimize application, it is critical to understand how Al content affects ZnS thin films deposited on glass substrates have optical characteristics. Preparation

* Corresponding author: gostaaagosy@hotmail.com
https://doi.org/10.15251/CL.2022.199.591

methods for ZnS thin films include electron beam deposition, thermal evaporation, sputtering, sol-gel, and chemical bath deposition [16-24]. The present work also deals with Al-doped ZnS films of various doping concentrations. A uniform doping distribution in ZnS is expected rather than a concentration gradient with a high lattice distortion. The optical properties of Al thin films deposited on soda-lime glass with ZnS substrates by PLD were investigated in this work.

2. Materials and methods

2.1. Preparation of AZS films

The PLD technique was used to prepare Al-doped ZnS films on glass substrates with dopant concentrations ranging from 0 to 6%. All reagents and chemicals were purchased from Sigma-Aldrich. $Zn_{1-x}Al_xS$ ($0 \leq x \leq 0.06$) samples were prepared by mixing ZnS and Al_2O_3 (99.99 % purity. The soda-lime glass was cleaned by immersing it in an ultrasound bath for ten minutes, the substrate was submerged in deionized water (DI). Ultrasonic agitation aided the process, the glass substrate was then rinsed and dried.

ZnS and ZnS: Al powder in the form of powders were mounted on a stepper-driven multi-target carrousel and exposed to the beam paths. The Al-dopant powder samples were pelletized and evaporated on glass substrates to prepare Al-doped ZnS films under controlled conditions. The system was then pumped down to a base pressure of 10^{-3} Torr.

The quartz crystal thickness monitor was placed just below the substrate holder to monitor the rate of deposition as well as film thickness. A shutter between the source and substrate controlled the deposition process and film thickness.

The deposition process studies were applied to estimate Neodymium-doped yttrium-aluminum-garnet (G) (Nd: $Y_3Al_2O_{12}$) Nd: YAG system. The Nd: YAG system was operated in TEM00 mode with fundamental and second harmonic outputs at 1064 and 532 nm. The laser was set to 100 mJ pulse energy, 500 pulses per second, 10 ns pulse repetition rate, and 6 Hz repetition frequency. The energy density or laser fluency was 2 J/cm^2. The laser energy density depends on the laser pulse energy and the recorded beam area. A computer system controls and monitors this process via an interface. The target laser source distance was 12.0 cm and the target substrate distance was 2.0 cm. The target was rotated as the laser rastered across a 0.5 cm^2 area. The 45° laser beams were focused on the sample **[25,26].**

3. Results and discussion

3.1. Absorption coefficient and energy gap

The absorption coefficient's value α was obtained from the formula given in Equation (1) [27]:

$$\alpha = \frac{1}{t} \ln(\frac{1}{T}) \quad (1)$$

where, t is the thickness of the film T is the transmission. The diagram of the absorption coefficient versus the wavelength, for the films depicted in Figure 1.a, the absorption coefficient for the undoped ZnS thin film decreased as well as an increase in the Al content.

The bandgap (E_g) The film values were determined using the Tauc relation [28]:

$$\alpha\, h\, f = A\,(h\, f - Eg)^2 \quad (2)$$

where A, h, f, and E_g are a constant, Planck's constant, frequency of the incidence radiation, and optical bandgap, respectively. The bandgap energy values of ZnS and AZS films were determined using the Tauc formula (2). Eg was calculated by drawing a straight line to the x-axis at the $(\alpha hf)^2 = 0$, as illustrated in Figure 1.b the linear dependence at the absorption edge substantiated by the $(\alpha hf)^2$ versus hf graph indicates that ZnS is a direct bandgap material. The Eg values of

ZnS and *AZS* films decreased significantly from 3.56 to 3.40 eV among as well as the increasing in the doping percentage of Al. These results are in agreement with the values reported for *ZnS* and *AZS* films in the published studies [29-31]. The bandgap The ZnS films' values were higher than those of *Al*-doped *ZnS* films.

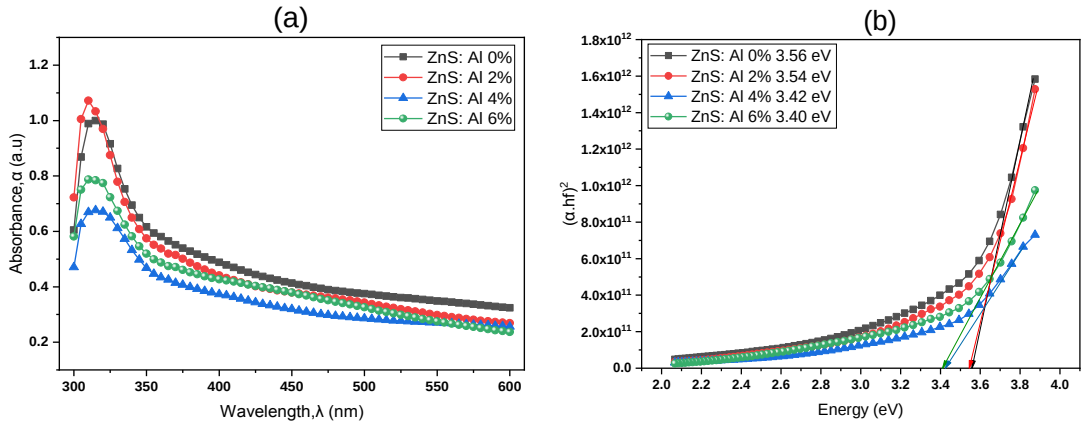

Fig. 1. The absorption coefficient spectrum (a), energy gap (b) for pure ZnS and AZS.

3.2. The linear optical parameters

The linear optical parameters including such oscillator energy (E_0), dispersion energy (E_d), and static refractive index (n_0) were calculated to investigate nonlinear optical susceptibility $\chi 3$ and nonlinear refractive index n_2. From Figure 2 (a) plots the refractive index $(n^2 - 1)^{-1}$ against the square of photon energy that was incident $(hv)^2$ for ZnS and AZS Table 1 displays films. The evaluated values of E_0 and E_d. The single-oscillator energy, E_0 values, obviously decrease with increasing *Al* content, and the same behavior is obtained for the energy gap, Eg. With the dispersion energy, E_d, values increased as the aluminum concentration increased. The width of the band tails (Urbach energy), which is used to characterize the degree of disorder in amorphous and semicrystalline materials, appears as a result of the evolution of localized states inside the forbidden band gap and can be estimated using the Urbach empirical rule [32]:

$$\alpha = \alpha_0 \exp\left(\frac{h\nu}{E_u}\right), \qquad \ln(\alpha) = \ln(\alpha_0) + \left(\frac{h\nu}{E_u}\right) \tag{3}$$

where α is the absorption coefficient, α_0 is constant, *hv* is the incident photon energy, and E_u is the Urbach energy. From Figure 4 (b) increasing the amount of *Al* in *ZnS* films raises the band tail or Urbach energy. The high density of localized states was implied by the large E_u values. The optical band gap and Urbach energy are evidently inversely proportional relationship. [33]:

$$(n^2 - 1)^{-1} = \frac{E_0}{E_d} - \frac{1}{E_0 E_d}(h\nu)^2 \tag{4}$$

$$n_0 = \sqrt{\left(1 + \frac{E_d}{E_0}\right)} \tag{5}$$

where E_d is the dispersion energy parameter, which measures the strength of the inter band optical transition, E_0 is the single-oscillator energy (energy gap average), and *hv* is the incident photon's energy. Plotting $(n^2 - 1)^{-1}$ versus $(hv)^2$ in Figure 4 (a), the plots give straight lines by fitting for liner spectra using Origin software, which intercepts the y-axis in a value equal to (E_0E_d), and the slope equal to ($-1/E_0E_d$).

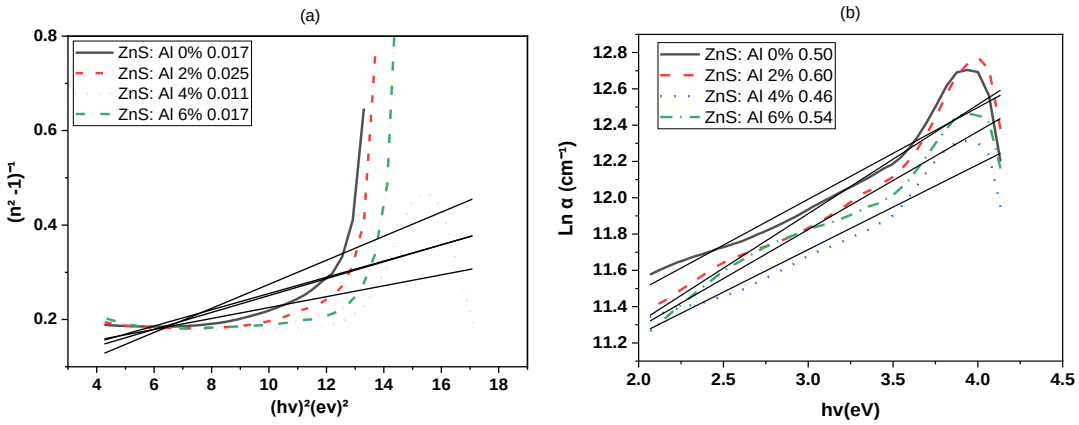

Fig. 2. Plotting $(n^2 - 1)^{-1}$ versus $(hv)^2$ figure (a), plot and linear fit of ln(α) against the photon energy hv for Al in ZnS thin films with different concentrations deposited at substrate figure (b).

The slope's defined as the ratio is the same as the values of Urbach energy when the linear part of ln α versus *hv* is plotted Figure 2.b. The obtained values of Urbach energy are listed in Table 1. It is discovered that increasing the amount of *Al* in *ZnS* films raises the band tail or Urbach energy from 0.50 to 0.54 eV. The high density of localized states was implied by the large E_u values. The optical band gap and Urbach energy were indeed evidently inversely proportional relationship [34].

$_0$Table 1. Single-oscillator energy, E_0, dispersion energy E_d, Urbach energy and refractive index, n_0, values according to Wemple and DiDomenico model.

Sample	E_0 (eV)	E_d (eV)	Urbach energy	n_0
ZnS: Al 0%	2.76	21.27	0.50	2.94
ZnS: Al 2%	2.19	18.25	0.60	3.05
ZnS: Al 4%	3.56	25.48	0.46	2.85
ZnS: Al 6%	2.65	22.14	0.54	3.05

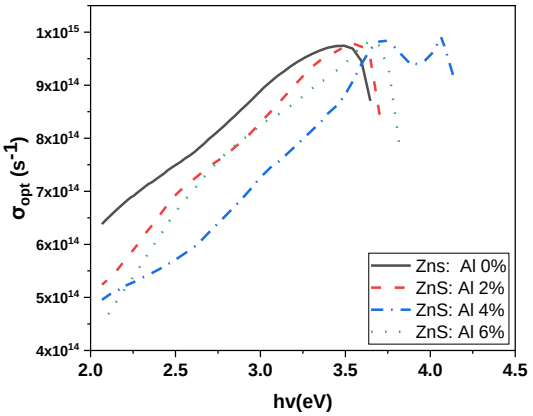

Fig. 3. Optical conductivity σ_{opt} versus incident photon energy hv.

The optical conductivity response caused by the motion of charge carriers in the electromagnetic waves that have been incident is referred to as σ_{opt} , calculated by used the equation below. Relationship between optical conductivity and a material's refractive index (n) and absorption coefficient [35]:

$$\sigma_{opt} = \frac{n.C.\alpha}{4\pi} \quad (6)$$

where *C* denotes the speed in aspects of light empty space. Figure 3 depicts the relationship between optical conductivity and Photon energy that is incident. As far as the content of the embedded *Al* increased, so did the optical conductivity. The incidence photon energy exciting electrons caused this increase in optical conductivity from the valence band to the conduction band at high photon energies. The establishment of new levels states in the band gap will establish from a material electrons move more easily broadening from the valence band to the nearest states, as a result of which there is a decrease in optical band gap.

3.3. The nonlinear optical parameters

The linear optical susceptibility χ^1 of the medium can be computed from the relation [36]:

$$\chi^1 = \frac{E_d / E_0}{4\pi} \quad (7)$$

Table 2 shows the evaluated linear optical susceptibility values and the nonlinear third order of the optical susceptibility χ^3 could be obtained from the linear refractive index n_0, dispersion energy E_d, and oscillator energy E_0 of the Wemple and DiDomenico single-oscillator model using Miller's rule, as evidenced by the following formula [37]:

$$\chi^3 = 6.82 \times 10^{-15} (E_d / E_0)^4 \quad (8)$$

The values of nonlinear refractive index n_2 are calculated in accordance with relation [38]:

$$n_2 = \frac{12\,\pi\,\chi^3}{n_0} \quad (9)$$

Table 2 shows the calculated values of n_2 and χ^3. The linear optical susceptibility, nonlinear third-order optical susceptibility, and nonlinear refractive index values are observed to increase as the *Al* content increases.

The samples' high nonlinear third-order susceptibility and nonlinear refractive index values indicate their suitability for use in various nonlinear optical and photonic devices and applications.

Table 2. Values of χ^1, χ^3 , and n_2 of the prepared AZS nanoparticles.

Sample	χ^1	$\chi^3 * 10^{-11}$ (e. s. u)	$n_2 * 10^{-10}$ (e. s. u)
ZnS: Al 0%	0.61	2.38	3.05
ZnS: Al 2%	0.66	3.28	4.05
ZnS: Al 4%	0.56	1.77	2.34
ZnS: Al 6%	0.66	3.28	4.05

3.4. Dielectric constant and Energy loss function

Real and imaginary parts of the dielectric constant are used to represent optical dielectric constants. $\varepsilon = \varepsilon_1 + i\,\varepsilon_2$. Real and imaginary parts of dielectric constant depend on the refractive index (n) and extinction coefficient (k) , based on the equation:

$$\mathcal{E}_1 = n^2 - k^2 \quad (10)$$

$$\mathcal{E}_2 = 2nk \quad (11)$$

Figure 4 depicts the dependent on $\mathcal{E}_1$ and $\mathcal{E}_2$ on photon energy. It has been noticed that the real part values of dielectric constant $\mathcal{E}_1$ Figure 4.a are greater than the imaginary part values of dielectric constant Figure 4.b $\mathcal{E}_2$, which is because $\mathcal{E}_1$ depends on the refractive index (*n*), whereas $\mathcal{E}_2$ depends on the extinction coefficient (*k*). As the *Al* concentration in *ZnS* films increases.

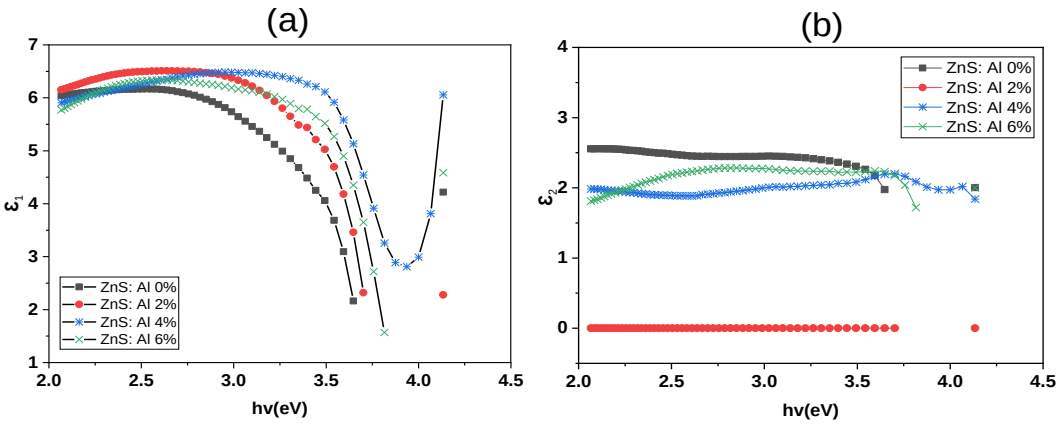

Fig. 4. Variation of optical dielectric constant with energy photon.

3.5. Energy loss function

The loss of energy from incident electromagnetic waves by electrons in a material or surface is related to the Volume energy loss function, and the Surface energy loss function (VELF) (SELF). The real and imaginary parts of dielectric constants ε_1 and ε_2 are related to the loss energy functions (VELF and SELF), as shown by the expression below. [39]:

$$VELF = \frac{\varepsilon_2}{\varepsilon_1^2+\varepsilon_2^2} \tag{12}$$

$$SELF = \frac{\varepsilon_2}{(\varepsilon_1+1)^2+\varepsilon_2^2} \tag{13}$$

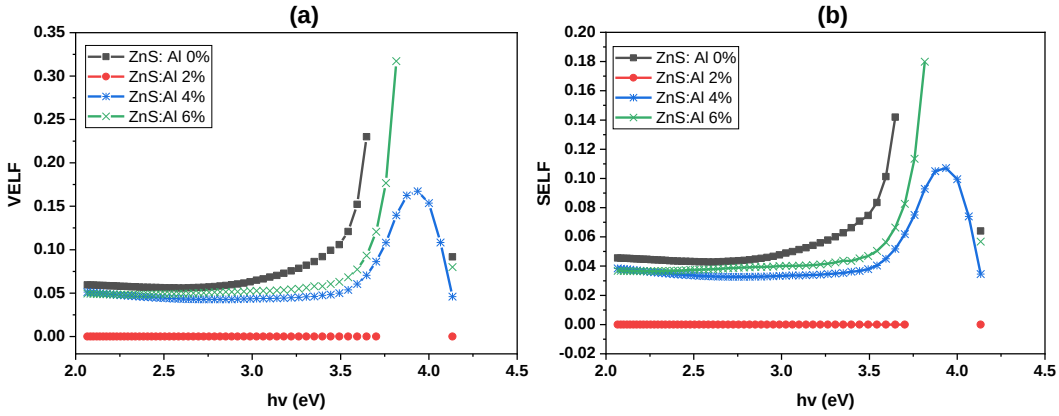

Fig. 5. Dependence of (a) VELF and (b) SELF on the photon energy hv for AZS nanoparticles.

Figure 5 depicts the relationship between *VELF* and *SELF* and incident energy (*hv*). It is discovered that the VELF and SELF values follow the same pattern, with no significant difference at higher and lower energy photons [40]. For each sample, the *SELF*-values are consistently lower than the *VELF* values. Along with the concentration of *Al* increases, the values of *SELF* and *VELF* decrease. The pure ZnS exhibited a different low *VELF* behavior at low energy.

4. Conclusion

ZnS and *AZS* Thin films were grown on soda-lime glass substrates using the PLD technique, with a reduction in the bandgap. Further, the bandgap energy values decreased significantly from 3.56 to 3.40 eV with an increase in the doping of *Al*. The optical conductivity increased as the amount of aluminum in the samples increased. The oscillator energy E_0, dispersion energy E_d, and static refractive index n_0 are calculated as dispersion parameters. The nonlinear optical susceptibility χ^3 and nonlinear refractive index n_2 were determined from the linear optical parameters by using the semiempirical relationship. With increasing nonlinear parameters χ^3 and n_2, *AZS* could be used for nonlinear optical applications. This study may open multiple horizons to achieve high-efficiency optoelectronic applications of *ZnS* thin films.

Acknowledgments

This work supported privately by the authors. There is no grant number or funding to declare. The authors appreciate the support and guidance of Dr. Taha Abdulhammed from Jouf University, Sakaka, Al-Jouf, SA.

References

[1] N. Kumar, S. Kumbhat, Carbon-Based Nanomaterials; (2016) pp. 189-236; https://doi.org/10.1002/9781119096122.ch5

[2] Y. Bouznit, Y. Beggah, A. Boukerika, A. Lahreche, F. Ynineb, Applied Surface Science, vol. 284 (2013), pp.936-941; https://doi.org/10.1016/j.apsusc.2013.03.155

[3] D. H. Hwang, J. H Ahn, K. N. Hui, K. S. Hui, Y. G. Son, Nanoscale Research Letters, 7:26,(2012); https://doi.org/10.1186/1556-276X-7-26

[4] U. Sarute, I. Yingyot, Renew. Sust. Energ. Rev., 55, (2016) 17-24; https://doi.org/10.1016/j.rser.2015.10.120

[5] J. Kennedy, P. P. Murmu, P. S Gupta, D. A. Carder, S. V. Chong, J. Leveneur, S. Rubanov, Mater. Sci. Semicond. Process, 26, (2014), 561-566; https://doi.org/10.1016/j.mssp.2014.05.055

[6] J. Cheng, D. Fan, H. Wang, B. Liu, Y. Zhang, H. Yan, Semicond. Sci. Technol., 18, (2003) 676-679; https://doi.org/10.1088/0268-1242/18/7/313

[7] J. Singh, and M. Rawat, J. Bioelectron Nanotechnol; 1(1): (2016) 5

[8] X. Fang, T. Zhai, U.K. Gautam, L. Li, L. Wu, L.; Y. Bando, D. Golberg, Prog. Mater. Sci., 56, (2011) 175-287; https://doi.org/10.1016/j.pmatsci.2010.10.001

[9] M. E. Pacheco, C. B. Castells, L. Bruzzone, Sens. Actuators B Chem. 238, (2017), 660-666; https://doi.org/10.1016/j.snb.2016.07.125

[10] X. Liu, Y. Yang, Q. Li, Z. Wang, X. Xing, Y. Wang, Sens. Actuators B Chem. 2018, 260, (2018), 1068-1075; https://doi.org/10.1016/j.snb.2018.01.121

[11] A. Attaf, A. Derbali, H. Saidi, H. Benamra, M. S. Aida, N. Attaf , H. Ezzaouia, L. Derbali, Physics Letters A, Volume 384, Issue 26, 18 September (2020), 126199; https://doi.org/10.1016/j.physleta.2019.126199

[12] B. Long, S. Cheng, H. Zhou, J. Liao, H. Zhang, H. Jia and H. Li, ECS Solid State Letters, 3, (2014), pp 140-P143; https://doi.org/10.1149/2.0041411ssl

[13] A. Jrad, T. Nasr and N. Turki-Kamoun, Journal of Materials Science: Materials in Electronics, 26, (2015), 8854-8862; https://doi.org/10.1007/s10854-015-3566-2

[14] Tulay Hurma, Materials Science-Poland 37 (4), (2019), 599-606; https://doi.org/10.2478/msp-2019-0072

[15] K. Nagamani, N. Revathi, P. Prathap, Y. Lingappa and K. R. Reddy, Current Applied Physics, 12, (2012), 380 – 384; https://doi.org/10.1016/j.cap.2011.07.031

[16] C. A. Bishop, Films and Foils; (2015); pp 301-331; https://doi.org/10.1016/B978-0-323-

29644-1.00016-5
[17] C. A. Bishop, Films and Foils; (2015); pp 289-299; https://doi.org/10.1016/B978-0-323-29644-1.00015-3
[18] H. Fujioka, Pulsed Laser Deposition (PLD), In Handbook of Crystal Growth; (2015); pp 365-397; https://doi.org/10.1016/B978-0-444-63304-0.00008-1
[19] D. Depla, S. Mahieu, J. E. Greene, In Handbook of Deposition Technologies for Films and Coatings; (2010); pp 253-296; https://doi.org/10.1016/B978-0-8155-2031-3.00005-3
[20] R. Reif, W. Kern, Plasma-Enhanced Chemical Vapor Deposition, In Thin Film Processes II;(2012); pp 525-564; https://doi.org/10.1016/B978-0-08-052421-4.50015-0
[21] D. Levy, M. Zayat, The Sol-Gel Handbook; Vol. 1-3, (2015); https://doi.org/10.1002/9783527670819
[22] V. Kumar, M. Saroja, M. Venkatachalam and S. Shankar, Synthesis and characterization of ZnS thin films by sol gel dip and spin coating methods, Int. J. Rec. Sci. Res. 6(11): (2015) 7377-7379
[23] M. R. De Guire, L. P. Bauermann, H. Parikh, J. Bill, Chemical Solution Deposition of Functional Oxide Thin Films; (2013); https://doi.org/10.1007/978-3-211-99311-8_14
[24] H. Benamra, H. Saidi, A. Attaf, M. S. Aida, A. Derbali, N. Attaf, Surfaces and Interfaces, 21, (2020), 100645; https://doi.org/10.1016/j.surfin.2020.100645
[25] M. H. EISA, Materials Science in Semiconductor Processing, Volume 110, (2020), 104966; https://doi.org/10.1016/j.mssp.2020.104966
[26] A. A. Kamil, N. A. Bakr , T. H. Mubarak, J. Al-Zanganawee, Digest Journal of Nanomaterials and Biostructures, Vol.16, (2021), p. 1219-1226
[27] R. Roy, V. S. Choudhary, M. K. Patra and A. Pandya, J. Optoelectron. Adv. Mater. 8(4): (2006), 1352- 1355.
[28] [17] VIPIN KUMAR, K.L.A. Khan, G. Singh and T.P. Sharma, Appl. Surf. Sci., (2007), 7, 253
[29] N. Bitri, K. Ben Bacha, Isabelle Ly, H. Bouzouita, M. Abaab, J Mater Sci: Mater Electron (2017) 28:734-744; https://doi.org/10.1007/s10854-016-5584-0
[30] G. M. Jigi, Tizazu Abza, Asnake Girma, Journal of Applied Biotechnology and Bioengineering, 2; 8(2): (2021) 55-58; https://doi.org/10.15406/jabb.2021.08.00252
[31] L.M. Abdul-Jabbar, Study the effect of annealing on optical and electrical properties of ZnS thin film prepared by CO2 laser deposition technique. Iraqi J. Laser. 13 (2014) 29-35
[32] T. A. Taha, and Ahmed Saleh, Applied Physics A 124.9 (2018): 1-12; https://doi.org/10.1007/s00339-018-2026-2
[33] S. H. Wemple, & M. DiDomenico Jr, Physical Review B, 3(4), (1971), 1338; https://doi.org/10.1103/PhysRevB.3.1338
[34] A. M. El Sayed, S. El-Sayed, W. M. Morsi, S. Mahrous, & A. Hassen, Synthesis, Polymer composites, 35(9), (2014), 1842-1851; https://doi.org/10.1002/pc.22839
[35] T. A. Taha, Z. Ismail, & E M. M. lhawary, Applied Physics A, 124(4), (2018), 1-13; https://doi.org/10.1007/s00339-018-1731-1
[36] H. N. Desai, J. M. Dhimmar, & B. P. Modi, Study of linear and non-linear optical parameters of zinc selenide thin film. Int J Eng Res Appl, 5(6), (2015), 117-122.
[37] F. A. Wahab, F. El-Diasty, & M. Abdel-Baki. Physics Letters A, 373(42), (2009), 3855-3860; https://doi.org/10.1016/j.physleta.2009.08.031
[38] T. A. Taha, Polymer Bulletin, 76(2), (2019). 903-918; https://doi.org/10.1007/s00289-018-2417-8
[39] H. A. Badran, M. F. AL-MUDHAFFER, Q. M. Hassan, & A. Y. Al-Ahmad, Chalcogenide Letters, 9(12), (2012), 483-493.
[40] A. A. Ebnalwaled, & A. Thabet, Synthetic Metals, 220, (2016), 374-383; https://doi.org/10.1016/j.synthmet.2016.07.006